OPTOELECTRONICS AND ADVANCED MATERIALS – RAPID COMMUNICATIONS Vol. 1, No. 6, June 2007, p. 287 - 293

Synthesis, structural and optical properties of nanocrystalline ZnO powders prepared by a PVA-polymer complex solution route

K. PATO, E. SWATSITANG, W. JAREONBOON, S. MAENSIRI*, V. PROMARAK[a]
Integrated Nanotechnology Research Center (INRC) and Small & Strong Solid Group (SSMG), Department of Physics, Faculty of Science, Khon Kaen University, Khon Kaen, 40002, Thailand
[a]*Advanced Organic Materials and Devices Laboratory, Department of Chemistry, Faculty of Science, Ubon Ratchathani University, Varinchamrap, Ubon Ratchathani 34190, Thailand*

This paper reports the synthesis, structural and optical properties of nanocrystalline ZnO powders with crystalline sizes of 26-69 nm (estimated by XRD) prepared by a PVA-polymer complex solution route (PCS). To obtain nanocrystalline ZnO powders, the precursor was calcined in air at temperatures between 500°C and 800°C for 2 h. The results of XRD and Raman spectroscopy confirmed the formation of polycrystalline wurtzite structure. The SEM observation revealed that the samples consisted of agglomerated nanoparticles with particle sizes of ~50-200 nm. The optical properties of the samples were also investigated by measuring the UV-vis absorption and photoluminescence spectra at room temperature. The synthesized powders exhibited the UV absorption below 400 nm (3.10 eV) with a well defined absorption peak at around 290 nm (4.28 eV). The estimated direct band gaps were obtained to 3.03, 3.07, 3.04, and 3.03 eV for the ZnO samples calcined at 500, 600, 700, and 800°C, respectively. All the samples exhibited room-temperature photoluminescence (PL) showing a strong UV emission broad band at ~ 390 nm (3.18 eV), a weak UV band at ~420 nm (2.96 eV), a week blue-green band at 484 nm (2.57 eV), and a green band at 530 nm (2.34 eV). The mechanisms responsible for photoluminescence of the samples were discussed.

(Received March 14, 2007; accepted April 25, 2007)

Keywords: Crystal structure, Growth from solutions, Nanomaterials, Zinc compounds, Semiconducting II-VI materials, Optical properties

1. Introduction

Zinc oxide (ZnO), a representative II–VI compound semiconductor, has received much attention over the last few years owing to its attractive properties such as wide and direct band gap of 3.37 eV, large exciton binding energy of 60 meV, good piezoelectric characteristics, chemical stability and biocompatibility. These suggest a wide range of possible practical applications, including field-emission displays, nano-photonic devices, piezoelectric transducers, varistors, phosphors, and transparent conducting films [1-11]. A variety of methods have been developed to prepare nanocrystalline ZnO with different particle morphologies and sizes, such as sol-gel method [12-14], thermal hydrolysis technique [15], spray pyrolysis [16], chemical vapor deposition on some substrates [17], low temperature wet-chemical methods [18-20], thermal evaporation of Zn [21], hydrothermal syntheses [22, 23], and solution-free mechanochemical reaction [24]. An excellent review of recent progress on processing, properties and applications of ZnO was recently published elsewhere [25]. Among these established synthesis methods, it is still critical to find alternative simple and cost effective routes to synthesize nanocrystalline ZnO by utilization of cheap, nontoxic and environmentally benign precursors.

In the present study, we present the synthesis and optical properties of nanocrystalline ZnO powders prepared by a polyvinyl alcohol (PVA) polymer complex solution route (PCS) [26]. This method utilizes water as a solvent instead of organic solvents. The advantages of this method include (i) use of small amount of organic substance and (ii) simple process without time-consuming polymerization and problem with treatment of a highly viscous polymeric resin. The synthesized ZnO samples were characterized by thermogravimetric-differential thermal analysis (TG-DTA), X-ray diffraction (XRD), Raman spectroscopy, UV-vis spectroscopy, and scanning electron microscopy (SEM). Photoluminescence properties of the samples were also investigated.

2. Experimental

In this study, $Zn(NO_3)_2$.$6H_2O$ (99.999% purity, Aldrich) and polyvinyl alcohol (PVA) (degree of polymerization ~1600, degree of hydrolysis 97.5-99.5 mol.%, Fluka) were used as the starting materials. In a typical procedure, 5 g (16.81 mmol) of $Zn(NO_3)_2$. $6H_2O$

was first dissolved in 100 ml de-ionized water under vigorous stir at room temperature (27°C) for 1 h to obtain homogeneous solution. Subsequently, 5 g of PVA was added to the nitrate solution under vigorous stir at 80°C for complete dissolution. The prolonged heating at 80°C over several hours produced a viscous organic gel without forming precipitation, and finally dried precursor was obtained. Throughout the whole process described above, no pH adjustment was made. The dried precursor was crushed into powder using mortar and pestle. In order to determine the temperature of possible decomposition and crystallization of the nanocrsytalline powders, the dried precursor was subjected to thermogravimetric-differential thermal analysis (TG-DTA) (Pyris Diamond TG-DTA, PerkinElmer Instrument). The crystallization seemed to occur at temperature above 480°C (Fig. 1). The dried precursor then was calcined in box-furnace at 500, 600, 700 and 800°C for 2 h in air. The final products obtained were white samples.

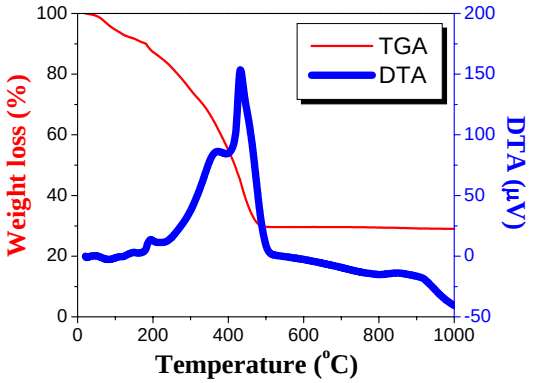

Fig. 1. TG-DTA curves of thermal decomposition of ZnO precursor at a heating rate of 10°C/min in static air.

The fine calcined particles were characterized for crystal phase identification by powder X-ray Diffraction (XRD) using a Philips X-ray diffractometer (PW3040, The Netherlands) with CuKα radiation (λ = 0.15406 nm). The Raman spectra were recorded at room temperature by using a triple spectrometer (Jobin Yvon/Atago-Bussan T-64000, France) with a liquid nitrogen cooled CCD detector for 800 s, in micro-mode. The Ar^+ laser beam with the excitation λ = 514.5 nm was focused under 90x microscope objective and the laser spot size was between 1 and 2 μm. Raman spectra were recorded in the 800–100 cm^{-1} range with a spectral resolution of 1 cm^{-1}. The particle size and external morphology of the fine calcined powders were characterized by scanning electron microscopy, SEM (LEO SEM 1450VP, UK). The optical absorption spectra were measured in the range of 200-800 nm using a UV-3101PC UV-VIS-NIR scanning spectrometer (Shimadzu, Japan). Photoluminescence measurement was carried out on a luminescence spectrometer (Perkin–Elmer LS-55B, PerkinElmer Instrument, USA) using a Xenon lamp as the excitation source at room temperature. The samples were dispersed in dichloromethane and the excitation wavelength used in PL measurement was 325 nm.

3. Results and discussion

The TG curve in Fig. 1 shows a major weight loss step from 194°C up to about 480 °C with no further weight loss observed up to 1000 °C. The weight loss is related to the combustion of organic matrix. The clear plateau formed between 480 °C and 1000 °C on the TG curve indicates the formation of nanocrystalline ZnO as decomposition product, as confirmed by XRD and Raman results shown in Fig. 2 and 3. On the DTA curve (Fig. 1) three exothermic effects were observed between 190 °C and 480 °C with a maximum strong peak at about 430 °C, indicating that the thermal events can be associated with the burnout of organic species involved in the precursor powders (organic mass remained from PVA), of the residual carbon or due to direct crystallization of nanocrystalline ZnO from the amorphous component.

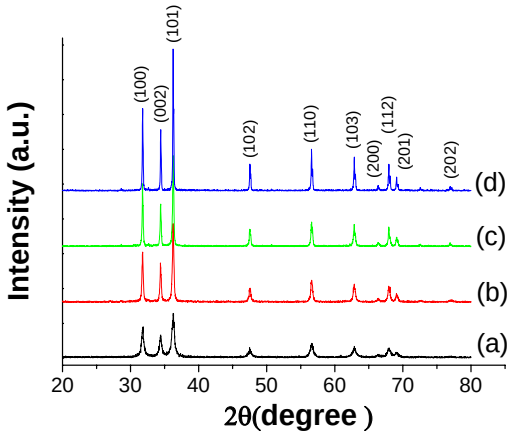

Fig. 2. XRD patterns of the dried precursor and nanocrystalline ZnO samples calcined in air for 2 h at (a) 500°C, (b) 600°C, (c) 700 °C, and (d) 800 °C.

The formation of ZnO after calcination at temperatures between 500 and 800°C is confirmed by XRD results. XRD patterns of all the samples in Figure 2 show typical peak patterns, which can be indexed as the ZnO wurtzite structure in the standard data (JCPDS, 36-1451). The wurtzite lattice parameters *a* and *c* calculated from the XRD spectra are (*a* = 0.3253(2) nm, *c* = 0.5207(2) nm), (*a* = 0.3248(2) nm, *c* = 0.5199(2) nm), (*a* = 0.3254(2) nm, *c* = 0.5208(2) nm) and (*a* = 0.3251(6) nm, *c* = 0.5202(6) nm) for ZnO samples calcined at 500, 600, 700 and 800°C, respectively. These values are close to those of lattice constants *a* = 0.3248(8) nm and *c* = 0.5206(6) nm in the standard data (JCPDS, 36-1451). The crystallite sizes of the powders were estimated from X-ray line broadening using Scherrer's equation [27]

(i.e. $D = 0.89\lambda/(\beta\cos\theta)$), where λ is the wavelength of the X-ray radiation, K is a constant taken as 0.89, θ is the diffraction angle. β is the full width at half maximum (*FWHM*)), and were obtained to be 26 ± 3, 28 ± 3, 49 ± 10 and 69 ± 15 nm for ZnO samples calcined at 500, 600, 700 and 800°C, respectively. It is seen from these results that the increasing calcination temperature leads to the stronger XRD intensity. This may also imply that increasing calcination temperature increases crystallinity of the synthesized ZnO samples. The particle sizes and lattice parameters are also summarized in Table 1.

Table 1. Average particle sizes from XRD line broadening, wurtzite lattice parameter a and c calculated from XRD spectra and the band gap (E_g) of the nanocrystalline ZnO samples calcined in air at different temperatures for 2h.

ZnO sample	Average particle size from XRD (nm)	Wurtzite parameters *a* and *c* (Å)	Estimated band gap (eV)
Calcined at 500°C	26 ± 3	*a* = 0.3253(2), *c* = 0.5207(2)	3..03
Calcined at 600°C	28 ± 3	*a* = 0.3248(2), *c* = 0.5199(2)	3.07
Calcined at 700°C	49 ± 10	*a* = 0.3254(2), *c* = 0.5208(2)	3.04
Calcined at 800°C	69 ± 15	*a* = 0.3251(6), *c* = 0.5202(6)	3.03

The formation of ZnO wurtzite structure in the synthesized ZnO samples was further supported by Raman spectra. The Raman spectra are sensitive to the crystal quality, structure defects and disorders of materials. ZnO in a Wurtzite structure belongs to the space group C_{6v}^4 ($P6_3mc$) with two formula units in the primitive cell, and all the atoms occupy C_{3v} sites [28]. The optical phonons at the Γ point of the Brillouin zone have the following irreducible representation [29]: $\Gamma_{opt} = 1A_1 + 2B_1 + 1E_1 + 2E_2$, where A_1 and E_1 modes are polar and split into transverse (TO) and longitudinal optical (LO) phonons, and they are all Raman and infrared active. The nonpolar E_2 modes are Raman active only and B_1 modes are Raman inactive. Fig. 3 shows the Raman spectra of the prepared ZnO samples in the 700–150 cm^{-1} range. The Raman spectra of all the ZnO samples exhibit a strong peak at ~ 437 cm^{-1}. The intensity of this Raman peak increases with increasing calcination temperature. The Raman spectrum of the ZnO sample calcined at 500°C shows only one strong peak at ~ 437.6 cm^{-1}, whereas the other samples exhibit other small peaks at ~330 and 580 cm^{-1}. The sample calcined at 700°C shows another peak at 380.7 cm^{-1}, while the sample calcined at 800°C exhibits two additional peaks at 379.1 and 407.4 cm^{-1}. Based on the well-established bulk ZnO data [18, 30-32], the strong peak at ~437 cm^{-1} is attributed to the optical phonon E_2 mode of the ZnO and is a characteristic Raman active peak for the wurtzite hexagonal phase of ZnO. The small peak at ~330 cm^{-1} is assigned to the second order Raman scattering arising from zone-boundary phonons, whereas small peaks at 380.7 cm^{-1} for the ZnO sample calcined at 700 °C and at 379.1 cm^{-1} for the ZnO sample calcined at 800 °C are attributed to A_1 symmetry with the TO mode. The other small peaks at 407.4 and ~580 cm^{-1} correspond to E_1 symmetries with TO and LO modes, respectively. It is generally accepted that the $E_1(LO)$ is related to the formation of structural defects in ZnO. Thus, the presence of $E_1(LO)$ indicates that oxygen vacancies or Zn interstitials were presented in the prepared samples [32]. It is worth noting that the presence of high intensity E_2 mode with the suppressed and low intensity $E_1(LO)$ peak indicates that the synthesized ZnO samples have good crystallinity with the wurtzite hexagonal crystal structure. These Raman results are consistent with the XRD measurements.

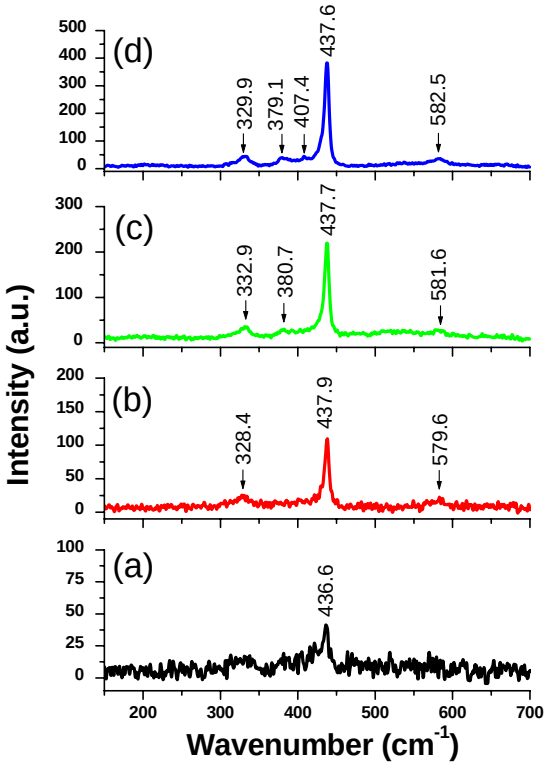

Fig. 3. Raman spectra of the dried precursor and nanocrystalline ZnO samples calcined in air for 2 h at (a) 500 °C, (b) 600 °C, (c) 700 °C, and (d) 800 °C.

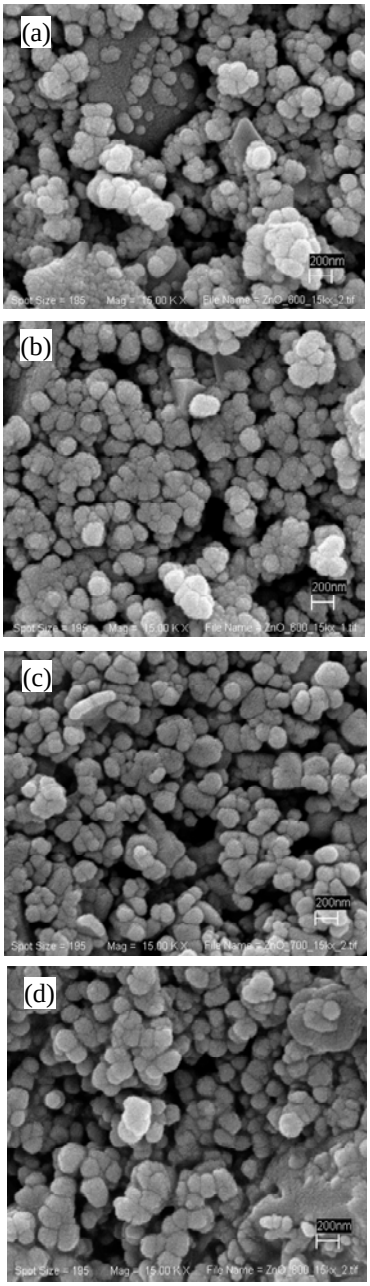

Fig. 4. SEM micrographs of the nanocrystalline ZnO samples calcined in air for 2h at (a) 500°C, (b) 600°C, (c) 700 °C, and (d) 800 °C.

The morphology of the samples was investigated by SEM. It is clearly seen from the SEM micrographs (Fig. 4) that the morphology of all the materials are agglomerated particles with sizes of ~50-200 nm. It is known from XRD results that the crystal sizes are 26 ± 3, 28 ± 3, 49 ± 10 and 69 ± 15 nm for ZnO samples calcined at 500, 600, 700 and 800°C, respectively. The large agglomerated particles seen in the SEM micrographs (Figure 4) may consist of these small particles (<100 nm). The agglomeration could be induced by densification resulting from the narrow space between particles due to the uniform distribution of oxidized metal anions in the three-dimensional polymeric network structure [33, 34].

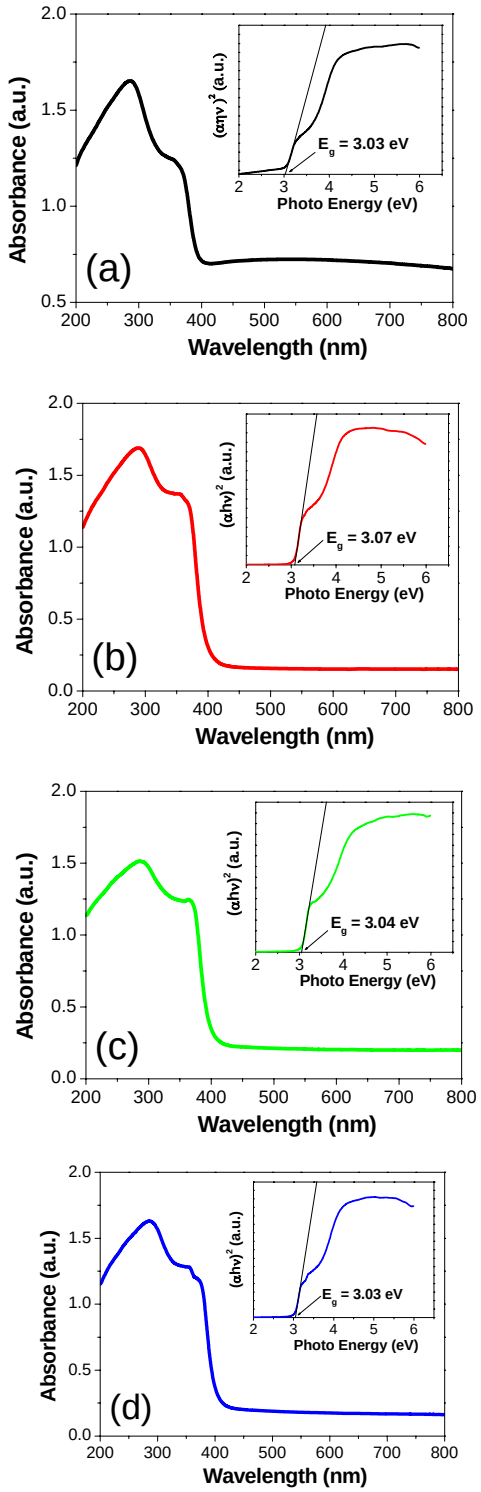

Fig. 5. Room temperature optical absorption spectra of the nanocrystalline ZnO samples calcined in air for 2h at (a) 500°C, (b) 600°C, (c) 700°C, and (d) 800°C. The insets are plots of $(\alpha h\nu)^2$ as a function of photon energy, E, for the ZnO samples.

The UV-visible absorbance spectra of all the samples shown in Fig. 5, exhibit a strong absorbance below 400 nm (3.10 eV) with a well defined absorption peak at around 290 nm (4.28 eV). The band edge for the ZnO samples appears at 370 nm (3.36 eV) which is close to that of typical pure ZnO phase reported in literatures [19, 35, 36]. The direct band gap energy (E_g) for the samples is determined by fitting the absorption data to the direct transition equation:

$$\alpha h\nu = E_D\left(h\nu - E_g\right)^{1/2}, \qquad (1)$$

where α is the optical absorption coefficient, $h\nu$ is the photon energy, E_g is the direct bandgap, and E_D is a constant [37]. Plotting $(\alpha h\nu)^2$ as a function of photon energy, and extrapolating the linear portion of the curve to absorption equal to zero as shown in the insets of Fig. 5, gives the values of the direct band gap (E_g) to be 3.03, 3.07, 3.04, and 3.03 eV for the ZnO samples calcined at 500, 600, 700, and 800°C, respectively. This value is lower than that of ~3.37 eV for ZnO reported in the literature [1]. Decrease in band gaps down to ~3.00 eV has been observed in Cd-doped ZnO alloy (i.e. $Zn_{1-x}Cd_xO$ with x = 0.07) [38] and in V-doped ZnO alloy (i.e. $Zn_{1-x}V_xO$ with x = 0.10) [39]. The low band gaps in the Cd-doped ZnO alloy and V-doped ZnO alloy are due to the low direct band gap of CdO (2.3 eV) [38] and the low direct band gap of VO groups such as V_2O_5 (2.3 eV) [40], respectively.

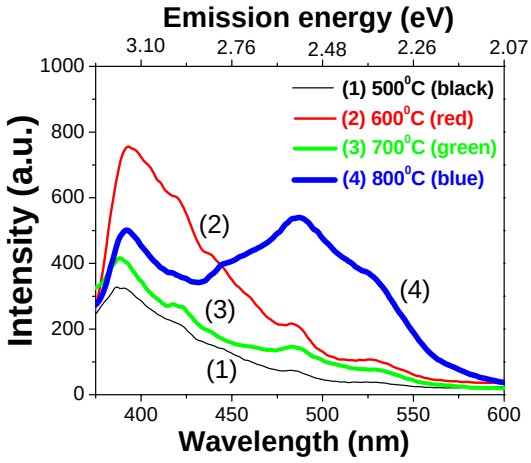

Fig. 6. Room temperature photoluminescence spectra of the synthesized nanocrystalline ZnO samples calcined in air for 2h at (a) 500°C, (b) 600°C, (c) 700°C, and (d) 800°C, under 325 nm light excitation.

The difference in the band gap values is one of the curious features of the literature on ZnO. Srikant and Clarke [41] investigated the optical band gap of ZnO single crystals at room temperature using a variety of optical techniques and reported three different E_g values of 3.1, 3.2, and 3.3 eV. They concluded that the room temperature band gap of ZnO was 3.3 eV, whereas the reports of apparent band gaps at 3.1 and 3.2 eV were due to the existence of a valence band-donor transition at 3.15 eV which can dominate the absorbance spectrum when the bulk, as distinct from the surface, of a single crystal is probed. In our previous work [19, 36], we also observed the low value of the direct band gap of 3.10 eV in nanocrystalline ZnO that had the mixture of nanoparticles with particle sizes of ~ 50-100 nm and nanorods with diameters of ~100-200 nm and 200-500 nm in length. Since there is no single crystal ZnO presented in the samples of the present study, the low value band gap of ~ 3.00 eV in our ZnO samples due to the presence of single crystal ZnO nanorods in the samples may be ruled out. We can not explain the mechanism responsible for low value band gap in our samples and further work is needed to achieve a thorough understanding.

Room temperature PL spectra of the nanocrystalline ZnO samples measured using an Xenon laser of 325 nm as excitation source are shown in Fig. 6. Similar PL spectra with different intensities were observed for the samples calcined at 500, 600 and 700°C, showing a strong UV emission broad band at ~ 390 nm (3.18 eV), a weak UV band at ~420 nm (2.96 eV), a week blue-green band at 484 nm (2.57 eV), and a green band at 530 nm (2.34 eV). The sample calcined at 600°C shows strongest PL intensity compared to those spectra of the samples calcined at 500 and 700°C. The sample calcined at 800°C also exhibits similar PL spectrum as obtained in other samples, except it consists of strong broad bands between 425 nm (2.92 eV) and 600 nm (2.02 eV) with the strongest blue-green band at 488 nm (2.54 eV). The strong UV emission corresponds to the exciton recombination related near-band edge emission of ZnO [42-44]. The weak blue-green emission is possibly due to surface defect in the ZnO samples [19, 36, 45]. The week green band emission corresponds to the singly ionized oxygen vacancy in ZnO, and this emission results from the recombination of a photo-generated hole with the singly ionized charge state of the specific defect [46-48]. The low intensity of the green emission may be due to the low density of oxygen vacancies during the preparation of the ZnO samples, whereas the strong room-temperature UV emission intensity should be attributed to the high purity with perfect crystallinity of the synthesized samples.

These differences in the PL results of the prepared nanocrystalline ZnO samples are possibly due to the differences in intrinsic defects, oxygen vacancies [42, 49] or zinc interstitials [50], which are highly located in band gap and act as sensitizing centers to trap electron from valence band to make a contribution to the photoluminescence. In poly- and nanocrystalline ZnO, oxygen vacancies are known to be the most common defects and usually act as radiative centers in luminescence process [18, 42, 44]. The stronger UV emission observed on the samples calcined at 600, 700 and 800°C compared to that of the sample calcined at 500°C may be due to their better crystallinity, while the weaker UV emission observed on the samples calcined at 700 and

800 °C compared to that of the sample calcined at 600°C may be due to their lower sensitizing centers. It is clear from XRD results that as the calcination temperature increases, the crystal size of ZnO samples becomes larger. As a results, the number of sensitizing centers decreases owing to reductions in both the ratio surface area and concentration of oxygen vacancies. Thus, this results in a decrease in PL intensity [18]. The strong blue-green emission observed on the 800 °C-calcined sample is possibly due to its highest crystallinity and lowest surface defects, while its broad green emission is attributed to the increase in density of oxygen vacancies during its calcination at the highest temperature of 800 °C.

4. Conclusions

Nanocrystalline ZnO powders have been synthesized by a simple PVA polymer solution. The PVA was used as a matrix for entrapment of zinc ions generating gelled precursor which resulted in nanocrystalline ZnO powders with crystalline sizes of 36-70 nm (estimated by XRD) after heat treatment of the gelled precursor at temperatures between 500-800°C for 2 h. The XRD and Raman results indicate that the all synthesized ZnO powders had the wurtzite structure. The morphology of the samples revealed by SEM shows that the powders consist of agglomerated nanoparticles with particle sizes of ~50-200 nm. The synthesized powders exhibited the UV absorption below 400 nm (3.10 eV) with a well defined absorbance peak at around 290 nm (4.28 eV). The estimated direct band gaps were in the range of 3.03-3.07 eV. Room-temperature PL spectra of the samples calcined at 500, 600, and 700°C showed a similar PL spectra consisting of a strong UV emission broad band at ~ 390 nm (3.18 eV), a weak UV band at ~420 nm (2.96 eV), a week blue-green band at 484 nm (2.57 eV), and a green band at 530 nm (2.34 eV). The sample calcined at 800°C also exhibited a similar PL spectrum but it has strong broad bands between 425 nm (2.92 eV) and 600 nm (2.02 eV) with the strongest blue-green band at 488 nm (2.54 eV). These differences in the PL results of the prepared nanocrystalline ZnO samples are attributed to the differences in intrinsic defects and oxygen vacancies which are highly located in band gap and act as sensitizing centers to trap electron from valence band to make a contribution to the photoluminescence.

Acknowledgements

The authors would like to thank the Department of Chemistry for providing UV-VIS-NIR facilities, the Faculty of Science Electron Microscopy Unit for providing SEM facilities. This work is supported by the Integrated Nanotechnology Research Center (INRC), Khon Kaen University.

References

[1] P. Zu, Z.K. Tang, G. K. L. Wong, M. Kawasaki, A. Ohtomo, H. Koinuma, Y. Segawa, Solid State Commun. **103**, 459 (1997).
[2] Z. K. Tang, G. K. L. Wong, P. Yu, M. Kawasaki, A. Ohtomo, H. Koinuma and Y. Segawa, Appl. Phys. Lett. **72**, 3270 (1998).
[3] D. C. Reynolds, D.C. Look, B. Jogai, C. W. Litton, T. C. Collins,W. Harsch, G. Cantwell, Phys. Rev. B **57**, 12151 (1998).
[4] B. M. Ataev, A. M. Bagamadova, V. V. Mamedov, A. K. Omaev, Mater. Sci. Eng. B **65**, 159 (1999).
[5] B. J. Jin, S.H. Bae, S. Y. Lee, S. Im, Mater. Sci. Eng. B **71**, 301 (2000).
[6] D. C. Look. Mater Sci Eng B **80**, 383 (2001).
[7] Z.W. Pan, Z. L. Wang, Science **291**, 1947 (2001).
[8] M. H. Huang,Y. Wu, H. Feick, N. Tran, E. Weber, P. D. Yang, Adv. Mater. **13**, 113 (2001).
[9] L. Vayssieres, K. Keis, A. Hagfeldt, S. E. Lindquist, Chem. Mater. **13**, 4395 (2001).
[10] S. H. Jo, J. Y. Lao, R. A. Farrer, T. Baldacchini, J. T. Fourkas, Appl. Phys. Lett. **83**, 4821 (2003).
[11] E. Ohshima, H. Ogino, I. Niikura, K. Maeda, M. Sato, M. Ito, T. Fukuda, J. Cryst. Growth **260**, 166 (2004).
[12] D. Vorkapic, T. Matsoukas, J. Am. Ceram. Soc. **81**, 2815 (1998).
[13] V. R. Palkar, Nanostruct. Mater. **11**, 369 (1999).
[14] Y. X. Li, K. J. Klabunde, Chem. Mater. **4**, 611 (1992).
[15] H. K. Park, D.K. Kim, C.H. Kim, J. Am. Ceram. Soc. **80**, 743 (1997).
[16] T. T. Kodas, Adv. Mater. **6**, 180 (1989).
[17] B. P. Zhang, N. T. Binh, K. Wakatsuki, Y. Segawa, Y. Yamada, N. Usami, M. Kawasaki, H. Koinuma, J. Phys. Chem. B **108**, 10899 (2004).
[18] Y. Du, M.-S. Zhang, J. Hong, Y. Sheen, Q. Chen, Z. Yin, Appl. Phys. A. 76, 171 (2003).
[19] S. Maensiri, P. Laokul, V. Promarak, J. Cryst. Growth **289**, 102 (2006).
[20] P-Y. Wu, J. Pike, F. Zhang, S-W Chan, Int. J. Appl. Ceram. Technol. 3, 272 (2006).
[21] G. Z. Shen, Y. Bando, Ch. J. Lee, J. Phys. Chem. B **109**, 10578 (2005).
[22] S.I. Hirano, Ceram. Bull. **66**, 1342 (1987).
[23] H. Zhang, D. R. Yang, D. S. Li, X.Y. Ma, S. Z. Li, D. L. Que, Cryst. Growth Des. **2**, 547 (2005).
[24] L. Shen, N. Bao, K. Yanagisawa, K. Domen, A. Gupta, C. A. Grimes, Nanotechnology **17**, 5117 (2006).
[25] S. J. Pearton, D. P. Norton, K. Ip, Y. W. Heo, T. Steiner, Prog. Mater. Sci. **580**, 293 (2005).
[26] S. Yamamoto, M. Kakihana, S. Kato, J. Alloy. Comp. **297**, 81 (2000).
[27] B. D. Cullity, S. R. Stock, Elements of X-ray Diffraction, 3nd ed.; Printice Hall: New Jersey (2001).
[28] T. C. Damen, S. P. S. Porto, B. Tell, Phys. Rev. **142**, 570 (1966).

[29] C. A. Arguello, D. L. Rousseau, S. P. S. Porto, Phys. Rev. **181**, 1351 (1969).
[30] J. M. Calleja, M. Cardona, Phys. Rev. B. **16**, 3735 (1977).
[31] F. Decremps, J. Pellicer-Porres, A. M. Saitta, J. C. Chervin, A. Polian, Phys. Rev. B. **65**, 092101 (2002).
[32] M. Rajalakshmi, A. K. Arora, B. S. Bendre, S. Mahamuni, J. Appl. Phys. **87**, 2445 (2000).
[33] Y. J. Kwon, K. H. Kim, C. S. Lim, K. B. Shim, J. Ceram. Proc. Res. **3**, 146 (2002).
[34] S. Maensiri, J. Sreesongmuang, C. Thomas, J. Klinkaewnarong, J. Magn. Magn. Mater. **301**, 422 (2006).
[35] M. Bouloudenine, N. Viart, S. Colis, A. Dinia, Chem. Phys. Lett. **397**, 73 (2004).
[36] S. Maensiri, P. Laokul, S. Phokha, J. Magn. Magn. Mater. **305**, 381 (2006).
[37] E. Ziegler, A. Heinrich, H. Oppermann, G. Stover, Phys. Status Solidi A **66**, 635 (1981).
[38] T. Makino, Y. Segawa, M. Kawasaki, A. Ohtomo, R. Shiroki, K. Tamura, Y. Yasuda, H. Koinuma, Appl. Phys. Lett. **78**, 1237 (2001).
[39] S. Maensiri, C. Masingboon, V. Promarak, S. Seraphin, Opt. Mater. (2007), doi:10.1016/j.optmat.2006.09.011. (in press)
[40] S. F. Cogan, N. M. Nguyen, S. J. Perrotti, R. D. Rauh, J. Appl. Phys. **66**, 1333 (1989).
[41] V. Srikant and D. R. Clarke, J. Appl. Phys. **83**, 5447 (1998).
[42] K. Vanheusden, W.L. Warren, C.H. Sesger, D.R. Tallant, J.A. Voigt, B.E. Gnage, J. Appl. Phys. **79**, 7983 (1996).
[43] S.C. Lyu, Y. Zhang, H. Ruh, H. Lee, H. Shim, E. Suh, C.J. Lee, Chem. Phys. Lett. **363**, 134 (2002).
[44] L. Bergman, X. B. Chen, J. L. Morrison, J. Huso, A. P. Purdy, J. Appl. Phys. **96**, 675 (2004).
[45] J. Wang, L. Gao, Solid State Comm. **132**, 269 (2004).
[46] S. Monticone, R. Tufeu, A.V. Kanaev, J. Phys. Chem. B **102**, 2854 (1998).
[47] Y. Li, G.S. Cheng, L.D. Zhang, J. Mater. Res. **15**, 2305 (2000).
[48] B.D. Yao, Y.F. Chan, N. Wang, Appl. Phys. Lett. **81**, 757 (2002).
[49] S. A. Studenikin, N. Golego, M. Cocievera, J Appl. Phys. **84**, 2287 (1998).
[50] J. Zhong, A. H. Kitai, P. Mascher, J. Electrochem. Soc. **140**, 3644 (1993).

*Corresponding author: sanmae@kku.ac.th;
santimaensiri@gmail.com